University of Huddersfield Repository

Kontogiorgos, Vassilis

Linear viscoelasticity of gluten: decoupling of relaxation mechanisms

Original Citation

Kontogiorgos, Vassilis (2017) Linear viscoelasticity of gluten: decoupling of relaxation mechanisms. Journal of Cereal Science, 75. pp. 286-295. ISSN 0733-5210

This version is available at http://eprints.hud.ac.uk/id/eprint/31931/

The University Repository is a digital collection of the research output of the University, available on Open Access. Copyright and Moral Rights for the items on this site are retained by the individual author and/or other copyright owners. Users may access full items free of charge; copies of full text items generally can be reproduced, displayed or performed and given to third parties in any format or medium for personal research or study, educational or not-for-profit purposes without prior permission or charge, provided:

- The authors, title and full bibliographic details is credited in any copy;
- A hyperlink and/or URL is included for the original metadata page; and
- The content is not changed in any way.

For more information, including our policy and submission procedure, please contact the Repository Team at: E.mailbox@hud.ac.uk.

http://eprints.hud.ac.uk/

LINEAR VISCOELASTICITY OF GLUTEN: DECOUPLING OF RELAXATION MECHANISMS

Vassilis Kontogiorgos

[a] Department of Biological Sciences, School of Applied Sciences, University of Huddersfield, HD1 3DH, Huddersfield, UK

***Corresponding author**

email: v.kontogiorgos@hud.ac.uk

Keywords: gluten, dynamics, stress relaxation, creep, poroelastic

Abstract

The influence of water content on the relaxation dynamics of mesoporous gluten networks has been explored in a wide range of temperatures. The systems were investigated in the linear viscoelastic region by means of stress relaxation, creep and numerical analysis of data. Time-temperature superposition principle and sticky reptation dynamics have been used to provide molecular interpretation of gluten relaxation. Overall, hydration influences relaxation behaviour of the system, which can be linked to changes in the secondary structure of gluten proteins with increase in water content. Relaxation spectra calculated with Tikhonov regularization revealed the remarkable influence of water on the long times relaxation processes of the material. Creep measurements and extraction of dynamic data with direct conversion of creep data *via* Laplace transform augmented the experimental timeframe of observations to low frequencies unattainable by standard frequency sweeps. The predominance of loss modulus at long times is attributed to migration of water within the nanopores of the structure. Samples also exhibit self-similar relaxation a characteristic of systems existing at a critical state. Two relaxation mechanisms can be distinguished: one arising from viscoelastic relaxation of protein chains and an additional stemming from poroelastic relaxation owing to migration of water in the system.

56 **1. Introduction**
57
58 Presence of nanocapillaries in materials gives rise to intricate thermodynamics, and
59 a range of different types of spatial confinement and pore-wall interactions can be used to
60 assist tuning the physical properties of soft matter. Gluten is a mesoporous biological
61 material with average pore diameter of about 5 nm and confinement of water in the
62 nanopores depresses melting point of confined water by more than 10 ^{o}C (Kontogiorgos
63 and Goff, 2006). It consists of more than fifty proteins with distinct structures resulting in
64 a particularly complex biological material that presents difficulties when is subjected to
65 rheological examination.
66 Viscoelasticity and macromolecular relaxations of hydrated biological structures is
67 largely determined by their water content, interactions with other constituents, pH and
68 ionic strength. Gluten viscoelasticity is frequently described with the "loops and trains"
69 model (LP-model) (Belton, 1999), which is essentially the Lodge model adapted to
70 gluten. In the Lodge model, junctions zone of the network break and reform with a
71 particular duration, as a result of transient binding between the polymer chains. The
72 transient binding in the LP-model is formed *via* hydrogen interactions between amino
73 acids of the polypeptide chains. The strength and extend of the interactions depends on
74 the level of hydration thus having direct influence on viscoelasticity. At low water
75 contents hydrogen interactions occur primarily between the amino acids of proteins while
76 as hydration increases the water-protein hydrogen bonding is enhanced.
77 It is well documented in the literature that hydration of gluten proteins induces
78 conformational changes to their structure. In particular, β-sheet to α-helix ratio increases
79 in response to hydration whereas at even higher hydration levels β-sheets are replaced

80 with β-turns (Almutawah et al., 2007; Belton et al., 1995; Popineau et al., 1994; Wang et
81 al., 2001; Wellner et al., 1996). The interplay of interactions between β-sheets, α-helices
82 and β-turns modulates the rigidity of the network as intermolecular hydrogen interactions
83 occurring between β-sheets will have greater number of neighbouring binding partners
84 compared to, for instance, α-helices or β-turns (Belton, 1999). Temperature-induced
85 conformational changes further complicate the landscape with additional formation of
86 intermolecular β-sheets by loss of α-helices or interchange of disulfide linkages on
87 heating (Georget and Belton, 2006). The cooperation of supramolecular forces,
88 temperature and time on gluten viscoelasticity have been recently put under rheological
89 scrutiny revealing that the importance of hydrogen bonding precedes over disulfide cross
90 links (Kontogiorgos et al., 2016). Additionally, in the mesoporous structure of gluten,
91 water is associated with the protein walls of the nanocapillaries with different strength
92 and molecular mobility (Bosmans et al., 2012; Kontogiorgos et al., 2007). Such structures
93 may allow water migration between neighbouring nanopores that further influences
94 viscoelasticity.

95 It is evident from the above discussion that water levels would play critical role in
96 the viscoelasticity of gluten networks and other similar hydrated biopolymer systems due
97 to chain conformational changes and water resettling within the pores of the structures. In
98 our previous investigations, we have focused on the influence of protein composition
99 (Kontogiorgos and Dahunsi, 2014) and supramolecular forces (Kontogiorgos et al., 2016)
100 on the relaxation dynamics of model gluten networks focusing, however, at one hydration
101 level. The aims of the present investigation are to build on our previous findings and by

102 using gluten as model system to explore the influence of hydration and decouple the
103 mechanisms that contribute to the relaxation dynamics in hydrated gluten.
104
105 **2. Materials and Methods**
106 *2.1 Materials and sample preparation*
107 Gluten was purchased from Sigma-Aldrich (Poole, UK) and the samples were
108 prepared at three levels of hydration: 70-30 (HW), 60-40 (MW), and 50-50 (LW) %w/w
109 where the first number corresponds to water content and the second to the protein solids
110 in the samples. Samples were labeled as HW, MW or LW for high, medium or low water
111 content, respectively. Following mixing, samples were left to hydrate for 30 min before
112 loading on to the rheometer as described elsewhere is detail (Kontogiorgos et al., 2007).
113 *2.2 Stress relaxation and creep measurements*
114 Stress relaxation measurements on shear were performed between 10–60 °C using
115 a rotational rheometer (Kinexus pro+, Malvern Instruments, Malvern, UK) equipped with
116 serrated plate geometry (25 mm diameter and 1 mm gap). The experimental settings have
117 been described in our previous work in detail (Kontogiorgos et al., 2016). Briefly, after
118 sample loading the specimens were left to relax for 15 min before measurements to
119 dissipate stresses that were created during loading. Shear strain amplitude sweep
120 experiments were then performed in the linear viscoelastic range of the samples (LVR) at
121 2% instantaneous strain for 30 min. Creep was conducted in the LVR of the samples in
122 the same temperature range and with the same geometry as the stress relaxation
123 measurements. An instantaneous stress of 20 Pa was applied and creep was carried out
124 for 30 min. A thin layer of low viscosity silicone oil (polydimethylsiloxane, Sigma-

125 Aldrich, St.Louis, MO) and a solvent trap were used to minimize moisture loss from the
126 edges of the geometry during measurement. Nonlinear regression was performed with
127 GraphPad Prism v.6 (Graph-Pad Software, SanDiego, USA).

128 *2.3 Computation of relaxation spectra*

129 Calculation of relaxation spectra was performed in MATLAB (v7.0 R14 Service
130 Pack 2, The Mathworks Inc., MA), as described previously (Kontogiorgos et al., 2016)
131 using Tikhonov regularization and the L-curve criterion to locate the optimum
132 regularization parameter, λ. Discretization of stress relaxation function was performed
133 between 0 and 30 min (minimum and maximum experimental time).

134 *2.4 Conversion of creep data to mechanical spectra*

135 Conversion of creep data to dynamic moduli proceeds with the application of
136 Laplace transform to the equation of motion of stress-controlled rheometers:

137 $$\mu \frac{d^2\gamma}{dt^2} + \int_0^t G(t-\tau) \frac{d\gamma}{d\tau} d\tau = \sigma_m(t) \qquad (1)$$

138 where μ is a positive constant representing instrumental inertia, which is given from
139 rheometer manufacturer, $\gamma(t)$ is the strain measured from creep test, $G(t)$ is the relaxation
140 modulus of the material and $\sigma_m(t)$ is the stress input given from the rheometer. Since the
141 term of Boltzmann superposition has the form of convolution, Laplace transform can
142 decompose the Laplace transform of creep compliance or equivalently that of relaxation
143 modulus because of the exact relation of:

144 $$s\tilde{J}(s) = \frac{1}{s\tilde{G}(s)} \qquad (2)$$

145 Numerical calculations proceed with Laplace transform of strain $\tilde{\gamma}(s)$ from experimental
146 data and conversion of $s\tilde{G}(s)$ to dynamic moduli (Kim et al., 2014; Kwon et al., 2016).
147

3. Results and Discussion

3.1 Stress relaxation measurements

The present investigation begins with exploration of the influence of water content on the stress relaxation behavior of gluten networks. Three levels of water were used and stress relaxation measurements were performed in the LVR between 10 and 60 ^{o}C for all samples (Fig. 1 a-c). The maximum (70% w/w) and minimum (50% w/w) hydration levels were chosen according to the levels of water that network is able to retain. At higher (*i.e.,* >70% w/w) or lower hydration levels (*i.e.,* <50 %w/w) water is either not retained in the structure or does not adequately hydrate proteins thus resulting in formation of anisotropic networks. Consequently, the present work reports on the entire range of hydration levels that can be used to create macroscopically isotropic gluten networks.

Hydration influences elasticity of the material particularly for LW samples where the network stiffens remarkably compared to its counterparts (Fig1 a, b *vs*. c). Temperature increase reduces relaxation modulus with diminishing influence beyond 50 ^{o}C at all hydration levels an observation that has been previously assigned to gluten network restructuring (Kontogiorgos and Dahunsi, 2014; Kontogiorgos et al., 2016; Tsiami, Bot and Agterof, 1997; Tsiami, Bot, Agterof, et al., 1997). The onset of the terminal regime is affected by temperature of the matrix where at temperatures above 30 ^{o}C the slow relaxation processes become particularly evident. The onset of long relaxation times is influenced by the rest time of the material on the geometry before measurement (Ng and McKinley, 2008), temperature, and on the specific molecular interactions within gluten (Kontogiorgos et al., 2016). Generally, onset time decreases

171 with temperature from about 800 s at 10 ^{o}C to 200 s at 60 ^{o}C whereas hydration levels do
172 not seem to play a role on the onset of slow relaxation modes. Early studies on the nature
173 of long processes have been attributed to the relaxation of the entire gluten network due
174 to its interconnectivity with disulfide linkages (Li et al., 2003) that could be generalized
175 as hindered motions of interacting polymer chains (Li et al., 2010). More recently
176 weakening of hydrogen bonding with temperature increase and water migration
177 (poroelastic relaxation) in the nanopores of the material have been also shown to play
178 determinant role for the long relaxation processes of this material (Kontogiorgos et al.,
179 2016). As it will be shown later, by following the slow modes with creep measurements,
180 poroelastic relaxation seems to be the determinant cause for the emergence and
181 development of the long relaxation events. The next step in our investigation was to
182 proceed with the construction of master curves of viscoelasticity for all samples using the
183 time temperature superposition principle to explore gluten network dynamics at
184 timeframes beyond those experimentally attainable.
185
186 *3.2 Time-temperature superposition and relaxation spectra*
187 Time-temperature superposition principle has been successfully applied on
188 several occasions before for gluten specimens (Dahesh et al., 2016; Kontogiorgos and
189 Dahunsi, 2014; Kontogiorgos et al., 2016; Tsiami, Bot, Agterof, et al., 1997). In the
190 present work, we have used the method of reduced variables to calculate the horizontal
191 shift factors (a_T=t/t_o) at reference temperature of 20 ^{o}C. Vertical shift factors are usually
192 needed when the material density changes during the course of rheological examination.
193 All samples studied are highly hydrated and density changes in the temperature range we

194 carried out the measurements will be dominated by changes in water density, which are
195 negligible between 10-60 ^{o}C (0.999-0.983 g/mL). In addition, the temperature
196 dependence of the vertical shift factor is generally weaker than the horizontal, thus it was
197 taken to be equal to unity. Construction of master curves extended the window of
198 observation for about four logarithmic cycles giving additional information on the fast
199 and slow relaxation processes of the samples (Fig. 2). In particular, hydration seems to
200 affect dramatically the fast relaxation processes ($\log (t/a_T) < \sim 1$) that represent the Rouse-
201 like modes of relaxation of the protein chains (Ng and McKinley, 2008) and essentially
202 vanish (*i.e.,* shift at shorter times) for MW and HW samples.

203 Utilization of the LT-model (Belton, 1999) provides molecular insights to the
204 behavior of the fast relaxation processes that is linked to changes in the protein structure
205 with increase in water content. At low hydration levels the individual protein chains
206 interact directly *via* hydrogen bonding, particularly of glutamine residues, creating
207 "trains". The "trains" behave as the spring of the Maxwell model that attempts to
208 instantaneously return the system to equilibrium. Increase in hydration results in changes
209 in secondary protein structure from α-helices to β-sheets, and with further increase of
210 hydration to β-turns, thus introducing water molecules between protein chains, as has
211 been described in the introduction. This state of affairs creates "loops" that weaken direct
212 hydrogen bonding between proteins thus decreasing its elasticity. These regions represent
213 the dashpot element in the Maxwell representation that exhibits viscous behavior.
214 Increase of the "viscous" elements in the system shift Rouse-like modes to much shorter
215 times that is not possible to observe with our current experimental protocol for samples
216 HW and MW in contrast to LW. Indeed, in our previous investigation Rouse-like modes

217 for MW samples have been observed at shorter times at about log $(t/a_T) < -2$ s
218 (Kontogiorgos et al., 2016). The power-law relaxation region is evident for all samples
219 (log $(t/a_T) > \sim 1$ s for the LW) and persists until the onset of the terminal regime.
220 Hydration influences the emergence of the terminal processes in the order of HW < MW
221 < LW with onset appearing at log (t/a_T) at ~ 5, 6 or 7, respectively (Fig 2) an observation
222 that was not evident from stress relaxation curves (Fig 1). In that case, it takes longer
223 time for proteins to “unzip” and relax to equilibrium state due to enhanced interactions in
224 the “train” regions as opposed to their “loop-rich” counterparts at higher hydration levels.
225 This behaviour can be formally described by utilizing tube dynamics and the
226 sticky reptation approach (Leibler et al., 1991; Xu and Craig, 2011). In the sticky Rouse
227 model the longest time for Rouse-like relaxation will be proportional to the number of
228 elastically active moieties of the protein chains and localized rearrangements of amino
229 acids. These are influenced by the number of disulfide cross-linking (Kontogiorgos et al.,
230 2016) and water content, as we have shown in the present investigation. In the transition
231 zone reptation commences and the modulus is mostly influenced by hydrogen-bonded
232 protein chains that do not form disulfide linkages. In this region hydrogen-bonded
233 segments of the chains, are the loci that store elastic energy. The continuous process of
234 engagement-disengagement of the transient binding associations results in absence of a
235 rubbery plateau and is attributed to the polydispersity of the material (Figure 2). Increase
236 in water content reduces the strength of the inter-protein interactions (*i.e.,* elastically
237 active associations) resulting in decrease of modulus and overall faster relaxation to
238 lower residual stresses (Figure 2). In the terminal region, proteins are released from the
239 tube with the remaining stress being proportional to the number of proteins that remain in

240 the tube. As it will be shown below, there is an additional mechanism that contributes to

241 the terminal relaxation.

242 To advance our understanding on the influence of temperature on the relaxation

243 mechanisms of the samples, the horizontal shift factors were plotted as a function of $T-T_o$

244 (Fig 2., top right inset). Up to 40 °C ($T-T_o$ = 20 °C) samples show gradual shift in a_T, as

245 temperature increase weakens hydrogen bonding, resulting in faster relaxation dynamics.

246 However, above 40 °C there is a step-change of about two logarithmic cycles in log a_T

247 particularly for MW and LW samples. Changes in the relaxation mechanisms at 40 °C has

248 been previously observed (Kontogiorgos et al., 2016) indicating temperature associated

249 structural changes in the network. Arrhenius relationship can be used to describe the

250 temperature dependence of a_T as:

251 $$\log a_T = \frac{E_a}{R}\left(\frac{1}{T} - \frac{1}{T_o}\right) \qquad (3)$$

252 where E_a is the relaxation activation energy and R the gas constant. Plotting log a_T *vs*. 1/T

253 (Fig 2, bottom left inset) results in activation energies of 53, 69 or 71 kJ/mol for HW,

254 MW or LW samples, respectively. Consequently, decrease in water content in the

255 samples increases the energy that is required for the chains to overcome the energy

256 barrier for molecular motion. This outcome is in line with the previous discussion on the

257 enhancement of intermolecular strength of protein interactions at low water contents due

258 to the proximity of the protein chains to each other.

259 The next step in the investigation dealt with the calculation of the continuous

260 relaxation spectra of the materials. The generalized function of the stress relaxation curve

261 is given by Fredholm integrals of the first kind as:

262 $$g(s) = \int_0^a K(s,t)H(t)dt, 0 \le s \le a \quad (4)$$

263 where $K(s, t)$ is the kernel $\exp(-t/s)$ that describes the decay, $g(s)$ is the relaxation
264 modulus, $G(t)$, and $H(t)$ is the continuous relaxation spectrum of the material. Integration
265 limits are between time zero and the maximum experimental time (α = 30 min). Curves
266 plotted in Fig 2 were analyzed using Tikhonov minimization yielding the relaxation
267 spectra of the networks (Fig 3). Relaxation spectra of gluten composites and other similar
268 biopolymer systems correspond to networks that exist in a *critical state* generally
269 revealing three characteristic regions: "glassy", power law and terminal (Gabriele et al.,
270 2001; Kontogiorgos et al., 2016; Meerts et al., 2016; Ng and McKinley, 2008). Polymeric
271 systems during sol-gel transition exhibit distinct rheological properties at the critical point,
272 one of them being self-similar relaxation (Winter, 2002). At the critical point, the
273 junction zones have not yet been established and return to the fluid state could be possible
274 with reversal of the gelation condition (*e.g.,* gelation reaction, temperature modulation
275 etc.). In the case of gluten, critical state is easily perceived due to the transient
276 interactions of hydrogen bonds that break and reform with a characteristic lifetime thus
277 making the system to exist in an interminable critical state. The entire network keeps its
278 solid-like character due to disulfide cross linking, absence of which results in fluid flow.
279 In addition, spectral analysis reveals some new striking features as water content
280 decreases in the system. Relaxation spectra present a minimum for HW samples at about
281 2×10^4 s that with reduction of water it gradually shifts outside our experimental window
282 ($>10^6$ s) (Fig 3) indicating that the long relaxation processes are highly dependent on the
283 water content in the networks. In our previous work, we have proposed two mechanisms
284 of relaxation in gluten, namely viscoelastic and poroelastic (Kontogiorgos et al., 2016).
285 The latter refers to the migration of water within the nanopores of the material. It has

286 been previously shown that modification of intermolecular interactions (Kontogiorgos et
287 al., 2016) or gluten composition (Kontogiorgos and Dahunsi, 2014) does not affect the
288 long relaxation processes of the material. Complementing past observations with those
289 from the current investigation, it emerges that the long relaxation processes are only
290 modified with changes in water content in the material. Relaxations caused by the
291 internal flow of solvent in the hydrogel have been previously described in the literature
292 for other hydrogels (Chan et al., 2012; Strange et al., 2013). It has been also suggested
293 that for whey protein gels viscoelastic relaxation should be considered at short times for
294 complete description of the relaxation processes (Mercadé-Prieto et al., 2016). This
295 analysis presents an important development in our understanding of the viscoelasticity of
296 this material as we have shown a clear relationship between water content and relaxation
297 behaviour. The mesoporous structure should be also taken into account as the physically
298 confined water in nanopores contributes to relieving the stress in the material.
299 Consequently, tuning the mechanical properties of gluten networks should mostly focus
300 on the water content in the structure.

301 As it transpired that water is the determinant factor for the mechanical properties
302 of the material, we proceeded to collect further evidence on the role of hydration on the
303 terminal relaxation processes. This was achieved with creep measurements in the LVR of
304 the material that are described in the next section.

305 *3.3 Creep measurements*

306 In the next step of our investigation we have undertaken creep measurements at
307 the two extremes of hydration (HW or LW) followed by conversion of creep data to
308 mechanical spectra. Creep measurements are more appropriate than dynamic and stress

309 relaxation for the measurement of long-term behavior of viscoelastic materials. In
310 addition, with conversion of creep curves to mechanical spectra we can retrieve
311 information about material properties from experimentally inaccessible frequencies.
312 Isothermal creep curves for LW and HW samples after application of instantaneous shear
313 stress in the LVR of the materials are presented in Fig 4.

314 Four distinct regions are distinguished, which is typical for polymeric materials
315 with structure. The initial strain of the curves corresponds to the elastic response of the
316 material after application of stress. The second region extends to about 0.02 s after the
317 application of the instantaneous stress where a peak is observed due to "ringing" (*i.e.,*
318 damped oscillations), as a result of the coupling of instrument inertia and sample
319 elasticity. In this region, the material begins to weaken under the effect of stress which is
320 temperature dependent with higher temperatures resulting in greater structural losses.
321 This region is followed by the steady state creep phase up to about 100 s. During this
322 phase, competing mechanisms of strain hardening and recovery may be present,
323 something that is particularly important for gluten polymers . In the final region beyond
324 100 s, strain curves for both samples show an upward trend. It is evident that HW
325 samples form weaker structures compared to LW counterparts at all temperatures as
326 higher protein hydration results in fewer direct intermolecular protein interactions and
327 greater molecular mobility of the chains. At long times the strain development is
328 described by (Kim et al., 2014; Kwon et al., 2016):

329 $$\gamma(t) \approx At^{\nu} \text{ for } t > t_{\max} \quad (5)$$

330 The parameter A and the terminal exponent v, are determined by regression analysis with
331 the data from the terminal regime ($t \sim t_{max}$). Additionally, in the terminal regime, raw data
332 of strain show:

333 $$\frac{dlog\gamma}{dlogt} \approx \nu \text{ for } t \sim t_{max} \quad (6)$$

334 When $v = 1$ the material behaves as a viscoelastic fluid whereas when $v = 0$ as a
335 viscoelastic solid. Terminal exponents as a function of temperature for HW and LW
336 samples range between 0 and 1 (Fig. 4b, inset) something that has been previously
337 observed for viscoelastic dispersions of xanthan (Kim et al., 2014). It is seen that higher
338 water contents and temperatures enhance the liquid-like character of the samples.
339 However, at temperatures above 40 °C a decrease of v is observed that is congruent with
340 the stress relaxation measurements. Denaturation of gluten proteins occurs over very
341 broad temperature range commencing at about 60 °C and continues unabated to 85 °C
342 due to heterogeneous protein composition (Leon et al., 2003). As creep and stress
343 relaxation measurements have been terminated at 60 °C, the networks should not exhibit
344 any measurable protein conformational changes in the window of temperatures we
345 operated. As a result, the observed changes in viscoelasticity should be attributed to the
346 mechanisms that have been described above.

347 The next step of the investigation was the conversion of creep data to dynamic
348 data yielding mechanical spectra with experimentally inaccessible angular frequencies
349 (0.0001 – 0.1 rad/sec) (Fig. 5). Conversion of creep data and recovery of mechanical
350 spectra is in agreement with previously published mechanical spectra of gluten with
351 conventional dynamic measurements on shear (Janssen et al., 1996; Meerts et al., 2016;
352 Tsiami, Bot, Agterof, et al., 1997). At long times (0.0001- 0.001 rad/s) loss modulus

353 dominates over storage something that is particularly noticeable in HW samples.
354 Combining information from three different rheological experimental treatments it
355 emerges that at long times the liquid like character controls the mechanical properties of
356 gluten composites. We attribute this behaviour to migration of water within the
357 nanoporous structure of the material that occurs in the terminal region of viscoelastic
358 relaxations. In addition, stress relaxation measurements that do not involve application of
359 stress for prolonged periods of time have also shown that the long relaxation peaks are
360 manipulated with changes in water content (Figure 4). At intermediate angular
361 frequencies (0.001-0.1 rad/s) storage modulus overtakes loss modulus whereas the latter
362 exhibits a peak. The reversible associations between protein chains prolong the relaxation
363 of the system and such systems exhibit two maxima in the $G''(\omega)$ function. The low
364 frequency peak is attributed to the disengagement of the proteins from the tube by
365 diffusion. This peak appears at frequencies $1/\tau$ where τ is the terminal relaxation time (Fig
366 1). Using data of Figure 1 onset of terminal relaxation ranges between 800 and 200 s
367 (depending on the temperature and water content) yielding angular frequencies between
368 0.0078 and 0.0314 rad/s, which is within the range of $G''(\omega)$ peaks presented in Figure 5.
369 The high frequency peak is generally difficult to be observed (~3 or 30 rad/s HW or LW
370 samples, respectively) and it attributed to dissipative processes of small peptides or
371 oligomers of gluten. At $\omega > 0.1$ rad/s viscoelastic moduli enter the power law region
372 which is a behaviour for systems existing in a critical gel state (Ng and McKinley, 2008).
373 In critical gels the storage and loss moduli should scale as (Winter, 2002):
374 $$G'(\omega) \sim \omega^n \text{ and } G''(\omega) \sim \omega^n \quad (7)$$

375 where n is the gel exponent and ω is the angular frequency. When $n \rightarrow 1$ the material
376 behaves as a soft gel whereas when $n \rightarrow 0$ it has characteristics of stiff network. Equation
377 7 indicates that at the gel point storage and loss moduli curves should run parallel to each
378 other *i.e.,* exhibiting the same exponent, n. Curve fitting between 1-10 rad/s yield n
379 values that are presented in Table 1. Close inspection of the table reveals that temperature
380 increase and/or decrease in moisture stiffens the network. These slopes agree particularly
381 well with previously observed in the literature as 0.22 (Meerts et al., 2016), 0.22-0.35
382 (Kontogiorgos et al., 2016) or 0.17 (Ng and McKinley, 2008). It can be seen that increase
383 in temperature augments the differences in the n values obtained from storage or loss
384 moduli, however, they are characteristically close (~0.3) particularly for the HW samples.
385 The behaviour of the exponents shows that gluten indeed displays characteristics of a
386 system existing near the sol-gel transition although disulfide cross-linking should be
387 responsible for the deviations from the theory (*i.e.,* exact agreement between n values).
388 The complexity of the relaxation processes can be also visualized with Cole-Cole plots of
389 G' *vs.* G'' (Figure 5a, inset). A semicircle in the Cole–Cole plot denotes a system with a
390 single relaxation time whereas if additional features appear in the right-hand part of the
391 curve (*e.g.,* shoulders or more arcs), they signify the existence of a longer relaxation
392 times with deviation from the ideal Maxwell behaviour, as is the case with our samples.
393 Taking everything into account, we could provide a highly idealized depiction of the
394 processes that are involved during gluten relaxation (Figure 6). At equilibrium (Figure
395 6a) gluten proteins are fully extended forming nanocapillaries that are able to confine
396 water. Water is physically confined with the aid of capillary forces but also because of
397 gluten-water interactions. Application of instantaneous strain (Figure 6b) disturbs

398 equilibrium and macromolecular relaxation begins in an attempt to reach equilibrium.
399 The very fast relaxation processes (Figure 6c) correspond to the elastically active
400 moieties of the protein chains and localized rearrangements of amino acids, as described
401 above. In the next stage, reptation of hydrogen-bonded segments of the protein chains
402 takes the lead and dominates over the rest of the processes further relieving the stress in
403 the material that is manifested with further decline in relaxation of modulus (Figure 6d).
404 In this part of the relaxation events, poroelastic relaxation also commences but does not
405 seem to play substantial role in the events. Finally, in the terminal regime confined water
406 disengages from the nanopores and migrates to neighbouring pores and poroelastic
407 relaxation is the dominant mechanism in an attempt to reach the initial equilibrium state
408 (Figure 6e).
409

410 **4. Conclusions**

411 Relaxation dynamics of mesoporous gluten networks as affected by water
412 content have been investigated by means of stress relaxation, creep and numerical
413 analysis of the ensuing data. Stress relaxation measurements in a wide range of
414 temperatures and application of time-temperature superposition principle enlarged the
415 experimental window of observation allowing construction of master curves of
416 viscoelasticity. Water content played critical role on relaxation dynamics affecting the
417 Rouse-like and terminal relaxation processes. Relaxation spectra revealed that the long
418 times relaxation processes can be only controlled by changes in water content. Probing
419 long-time relaxation processes with creep measurements conversion of the curves to
420 mechanical spectra allowed assessing experimentally inaccessible frequencies. The

networks present characteristics of systems that exist in a critical state throughout all the functionally relevant temperatures and hydration levels. Combination of rheological data revealed that the long relaxation processes should be associated with water migration in the pores of the structure. As a result, the mechanisms of gluten network relaxation can be separated into viscoelastic due to protein relaxation and poroelastic due to water migration in the nanopores.

Acknowledgements: The author wishes to thank Prof. Kwang Soo Cho, Kyungpook National University for the conversion of creep data to mechanical spectra.

445

446 **5. References**

447 Almutawah, A., Barker, S.A., Belton, P.S., 2007. Hydration of Gluten: A Dielectric,
448 Calorimetric, and Fourier Transform Infrared Study. Biomacromolecules 8, 1601-1606.

449 Belton, P.S., 1999. On the elasticity of wheat gluten. Journal of Cereal Science 29, 103-
450 107.

451 Belton, P.S., Colquhoun, I.J., Grant, A., Wellner, N., Field, J.M., Shewry, P.R., Tatham,
452 A.S., 1995. FTIR and NMR studies on the hydration of a high-Mr subunit of glutenin.
453 International Journal of Biological Macromolecules 17, 74-80.

454 Bosmans, G.M., Lagrain, B., Deleu, L.J., Fierens, E., Hills, B.P., Delcour, J.A., 2012.
455 Assignments of proton populations in dough and bread using NMR relaxometry of starch,
456 gluten, and flour model systems. Journal of Agricultural and Food Chemistry 60, 5461-
457 5470.

458 Chan, E.P., Deeyaa, B., Johnson, P.M., Stafford, C.M., 2012. Poroelastic relaxation of
459 polymer-loaded hydrogels. Soft Matter 8, 8234-8240.

460 Dahesh, M., Banc, A., Duri, A., Morel, M.-H., Ramos, L., 2016. Spontaneous gelation of
461 wheat gluten proteins in a food grade solvent. Food Hydrocolloids 52, 1-10.

462 Gabriele, D., de Cindio, B., D'Antona, P., 2001. A weak gel model for foods. Rheologica
463 Acta 40, 120-127.

464 Georget, D.M.R., Belton, P.S., 2006. Effects of Temperature and Water Content on the
465 Secondary Structure of Wheat Gluten Studied by FTIR Spectroscopy.
466 Biomacromolecules 7, 469-475.

467 Janssen, A.M., van Vliet, T., Vereijken, J.M., 1996. Rheological behaviour of wheat
468 glutens at small and large deformations. Comparison of two glutens differing in bread
469 making potential. Journal of Cereal Science 23, 19-31.

470 Kim, M., Bae, J.-E., Kang, N., Soo Cho, K., 2014. Extraction of viscoelastic functions
471 from creep data with ringing. Journal of Rheology 59, 237-252.

472 Kontogiorgos, V., Dahunsi, O.S., 2014. Relaxation dynamics in hydrated gluten networks.
473 Journal of Cereal Science 59, 101-108.

474 Kontogiorgos, V., Goff, H.D., 2006. Calorimetric and microstructural investigation of
475 frozen hydrated gluten. Food Biophysics 1, 202-215.

476 Kontogiorgos, V., Goff, H.D., Kasapis, S., 2007. Effect of aging and ice structuring
477 proteins on the morphology of frozen hydrated gluten networks. Biomacromolecules 8,
478 1293-1299.

479 Kontogiorgos, V., Shah, P., Bills, P., 2016. Influence of supramolecular forces on the
480 linear viscoelasticity of gluten. Rheologica Acta, 1-9.

481 Kwon, M.K., Lee, S.H., Lee, S.G., Cho, K.S., 2016. Direct conversion of creep data to
482 dynamic moduli. Journal of Rheology 60, 1181-1197.

483 Leibler, L., Rubinstein, M., Colby, R.H., 1991. Dynamics of reversible networks.
484 Macromolecules 24, 4701-4707.

485 Leon, A., Rosell, C.M., De Barber, C.B., 2003. A differential scanning calorimetry study
486 of wheat proteins. European Food Research and Technology 217, 13-16.

487 Li, J., Ngai, T., Wu, C., 2010. The slow relaxation mode: from solutions to gel networks.
488 Polymer Journal 42, 609-625.

489 Li, W., Dobraszczyk, B.J., Schofield, J.D., 2003. Stress relaxation behavior of wheat
490 dough, gluten and gluten protein fractions. Cereal Chemistry 80, 333-338.

491 Meerts, M., Cardinaels, R., Oosterlinck, F., M. Courtin, C., Moldenaers, P., 2016. The
492 Interplay Between the Main Flour Constituents in the Rheological Behaviour of Wheat
493 Flour Dough. Food and Bioprocess Technology, 1-17.

494 Mercadé-Prieto, R., Lopez, J., Chen, X.D., 2016. Poroelastic relaxation indentation of
495 whey protein hydrogels. Food Hydrocolloids 54, Part B, 221-226.

496 Ng, T.S.K., McKinley, G.H., 2008. Power law gels at finite strains: The nonlinear
497 rheology of gluten gels. Journal of Rheology 52, 417-449.

498 Popineau, Y., Bonenfant, S., Cornec, M., Pezolet, M., 1994. A Study by Infrared
499 Spectroscopy of the Conformations of Gluten Proteins Differing in their Gliadin and
500 Glutenin Compositions. Journal of Cereal Science 20, 15-22.

501 Strange, D.G.T., Fletcher, T.L., Tonsomboon, K., Brawn, H., Zhao, X., Oyen, M.L., 2013.
502 Separating poroviscoelastic deformation mechanisms in hydrogels. Applied Physics
503 Letters 102, 031913-031914.

504 Tsiami, A.A., Bot, A., Agterof, W.G.M., 1997. Rheology of mixtures of glutenin
505 subfractions. Journal of Cereal Science 26, 279-287.

506 Tsiami, A.A., Bot, A., Agterof, W.G.M., Groot, R.D., 1997. Rheological properties of
507 glutenin subfractions in relation to their molecular weight. Journal of Cereal Science 26,
508 15-27.

509 Wang, Y., Belton, P.S., Bridon, H., Garanger, E., Wellner, N., Parker, M.L., Grant, A.,
510 Feillet, P., Noel, T.R., 2001. Physicochemical Studies of Caroubin: A Gluten-like Protein.
511 Journal of Agricultural and Food Chemistry 49, 3414-3419.

512 Wellner, N., Belton, P.S., Tatham, A.S., 1996. Fourier transform IR spectroscopic study
513 of hydration-induced structure changes in the solid state of œâ-gliadins. Biochemical
514 Journal 319, 741.

515 Winter, H.H., 2002. The Critical Gel, in: Borsali, R., Pecora, R. (Eds.), Structure and
516 Dynamics of Polymer and Colloidal Systems. Springer Netherlands, Dordrecht, pp. 439-
517 470.

518 Xu, D., Craig, S.L., 2011. Scaling Laws in Supramolecular Polymer Networks.
519 Macromolecules 44, 5465-5472.
520

521

522

523

524

525

526

527

528

529

530

531

532

533

534

535

536

537

538

539 **FIGURE LEGENDS**

540 **Figure 1:** Double logarithmic plots of stress relaxation curves between 10 and 60 °C for
541 all gluten samples: a) HW, b) MW, and c) LW.

542 **Figure 2:** Double-logarithmic plots of master curves of stress relaxation modulus against
543 reduced time at T_o = 20 °C for all samples. Top right inset shows the temperature
544 dependence of shift factors (a_T) plotted against T-T_o. Bottom left inset shows the
545 calculations of the activation energy in semi-logarithmic plots of $\log a_T$ *vs.* 1/T.

546 **Figure 3:** Double-logarithmic plots of relaxation spectra calculated using data from
547 master curves (Fig. 2).

548 **Figure 4:** Double logarithmic plots of creep curves between 10 and 60 °C for gluten
549 samples: a) HW, and b) LW, inset shows the development of terminal exponent v with
550 temperature.

551 **Figure 5:** Mechanical spectra obtained by direct conversion of creep curves in Figure 4.
552 Filled or open symbols indicate storage or viscous modulus, respectively. a) HW
553 samples: square at 20 °C, and triangle at 40 °C, Top-right inset: Cole-Cole plots for LW
554 samples, b) LW samples: circle at 30 °C and diamond at 50 °C.

555 **Figure 6:** Idealized depiction of the processes that are involved in gluten relaxation.
556 Strands (brown zig-zag lines) represent gluten walls that form nanocapillaries that
557 confine water (blue circles). a) Equilibrium before application of strain, b) application of
558 instantaneous strain, c) in the first stage, fast relaxation processes correspond mostly to
559 the elastically active protein moieties, d) in the second stage, continuous reptation of
560 hydrogen-bonded segments of the protein chains reduces further relaxation modulus, and

561 e) in the final stage, poroelastic relaxation is the dominant mechanism. Confined water

562 may also migrate to neighbouring pores whereas gluten proteins are mostly relaxed.

563

564

565

566

567

568

569 **TABLES**

570 **Table 1:** Slopes of the curves of Figure 5 between 1-10 rad/s that represent the gel
571 exponent *n* at all temperatures for HW and LW.

	HW		**LW**	
Temperature (^oC)	Slope G´(ω)	Slope G´´(ω)	Slope G´(ω)	Slope G´´(ω)
10	0.28	0.33	0.28	0.40
20	0.27	0.33	0.23	0.36
30	0.25	0.28	0.20	0.36
40	0.18	0.30	0.22	0.38
50	0.17	0.33	0.25	0.35
60	0.17	0.29	0.18	0.36

572

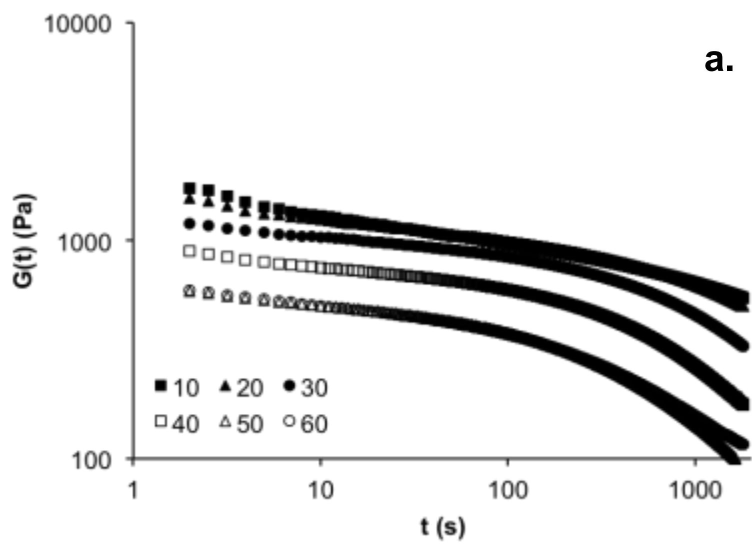
10000
1000
100
G(t) (Pa)
1
10
100
1000
t (s)
a.
10
20
30
40
50
60

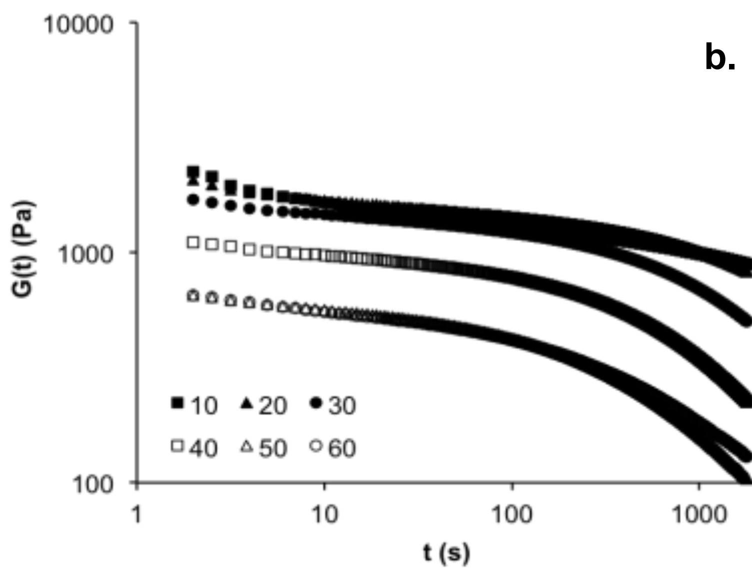
10000
1000
100
G(t) (Pa)
1
10
100
1000
t (s)
b.
10
20
30
40
50
60

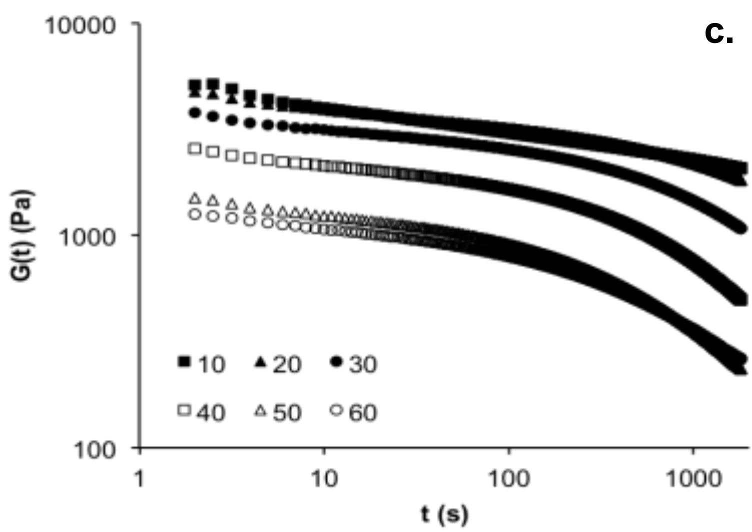
10000
1000
100
G(t) (Pa)
1
10
100
1000
t (s)
c.
10
20
30
40
50
60

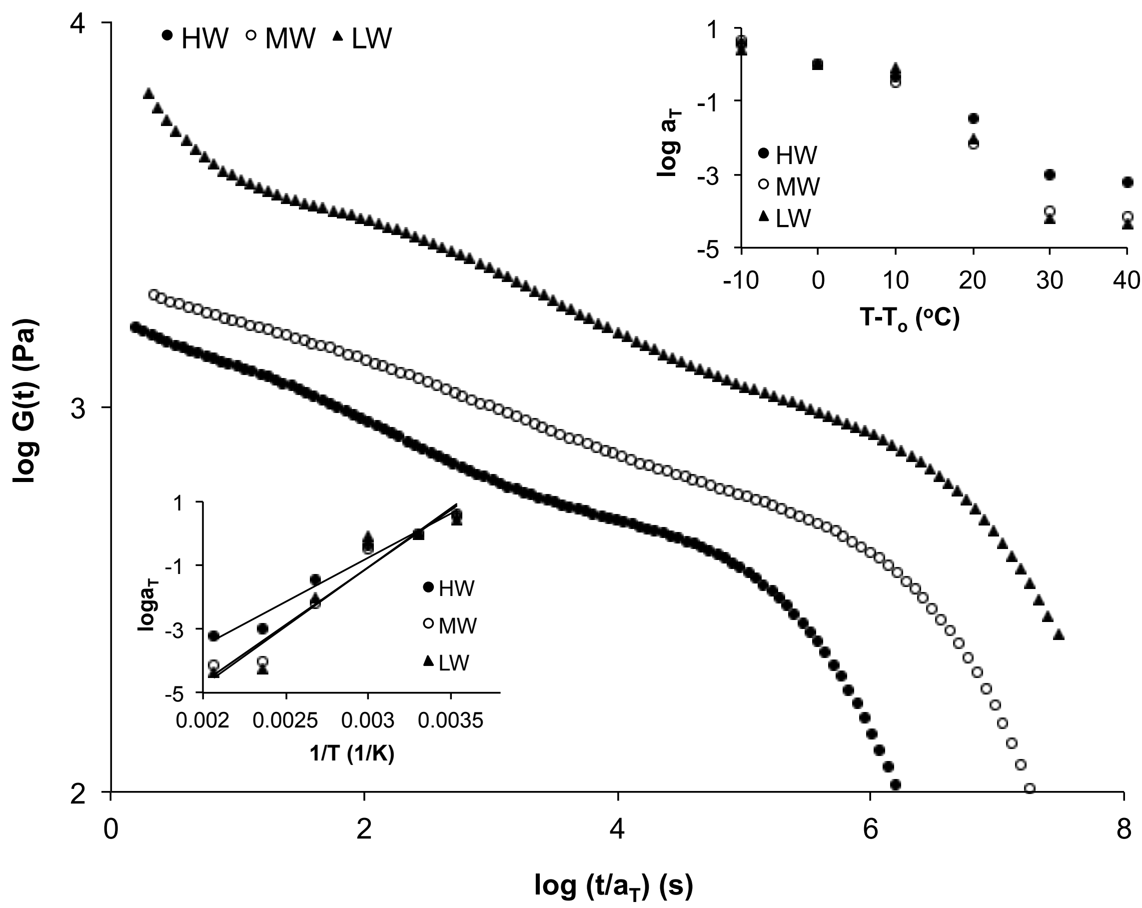

HW
MW
LW
log G(t) (Pa)
log (t/a$_T$) (s)
log a$_T$
T-T$_o$ (°C)
loga$_T$
1/T (1/K)

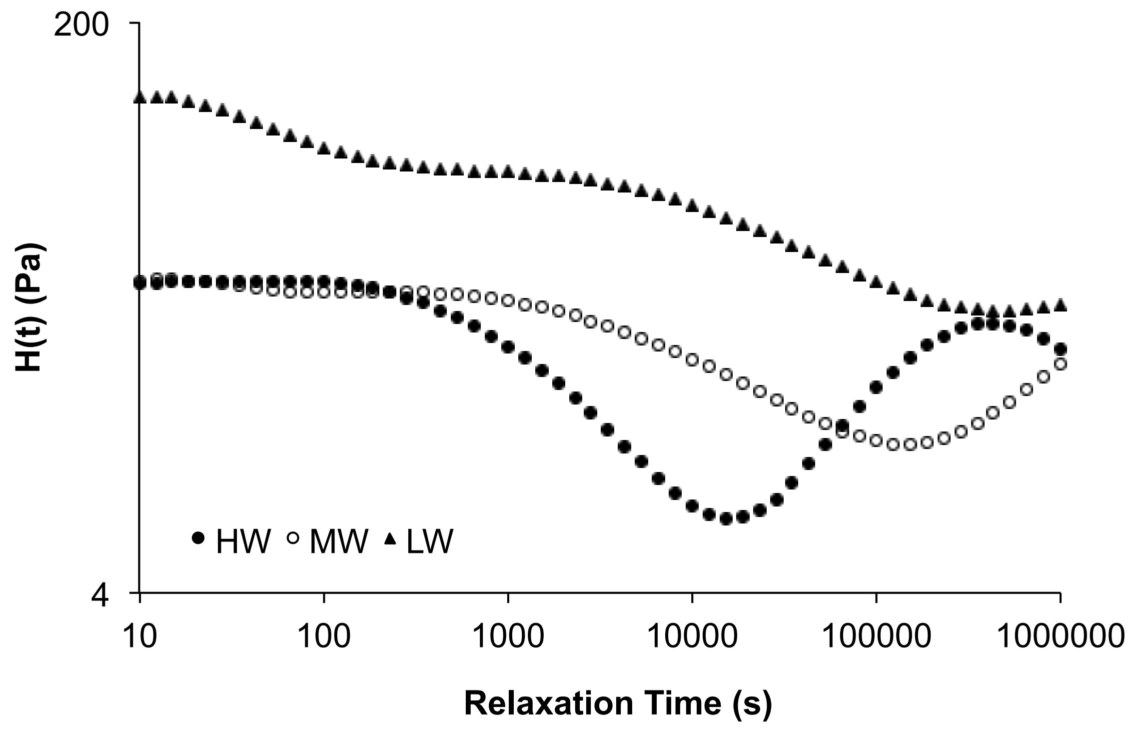

200
4
H(t) (Pa)
10
100
1000
10000
100000
1000000
Relaxation Time (s)
HW
MW
LW

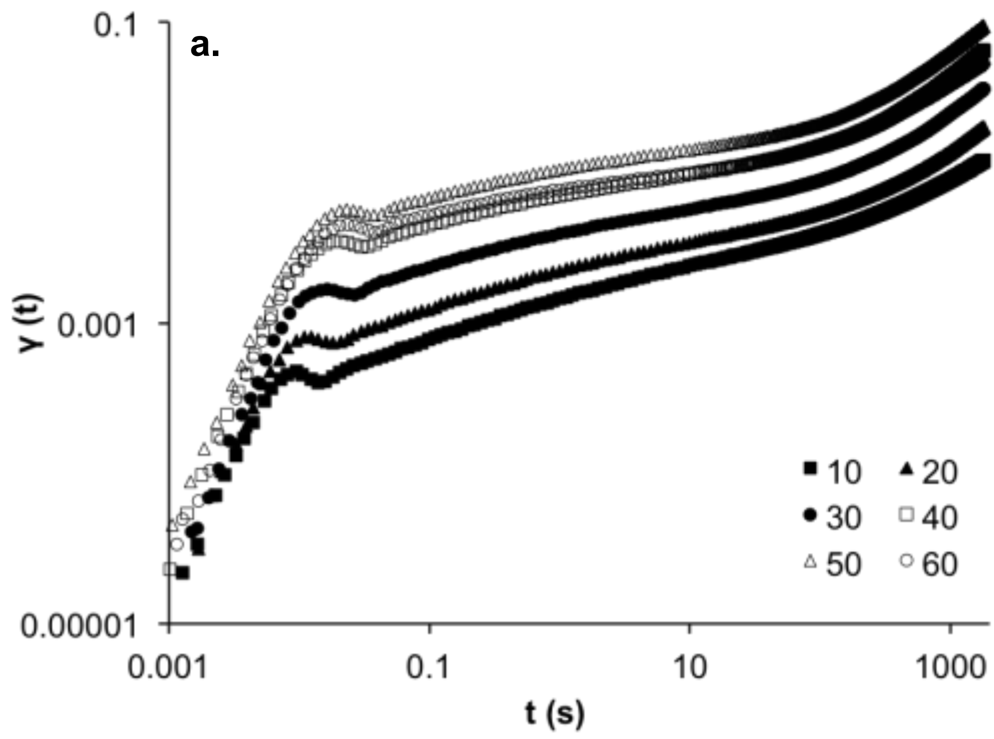
a.
0.1
0.001
0.00001
γ (t)
0.001
0.1
10
1000
t (s)
10
20
30
40
50
60

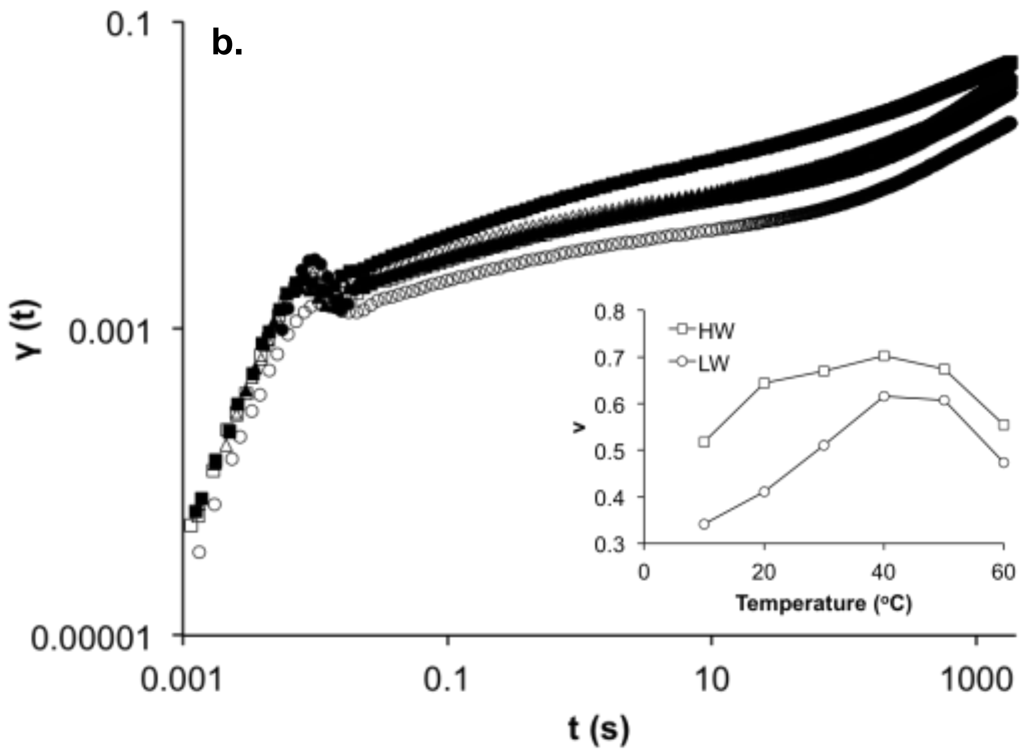
b.
0.1
0.001
0.00001
γ (t)
0.001
0.1
10
1000
t (s)
HW
LW
v
0.8
0.7
0.6
0.5
0.4
0.3
0
20
40
60
Temperature (°C)

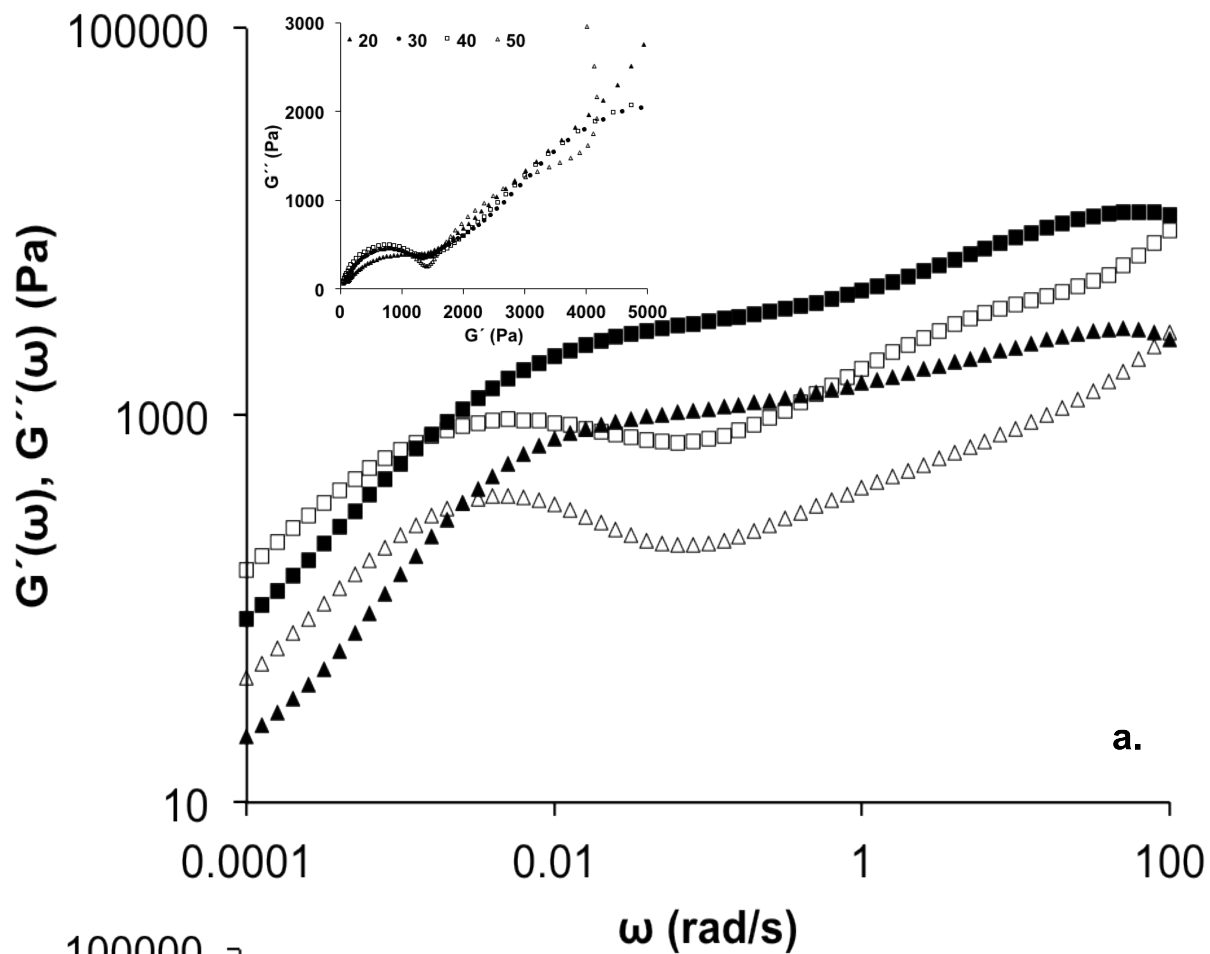
100000
1000
10
0.0001
0.01
1
100
G´(ω), G´´(ω) (Pa)
ω (rad/s)
a.
3000
2000
1000
0
0
1000
2000
3000
4000
5000
G´´ (Pa)
G´ (Pa)
20
30
40
50

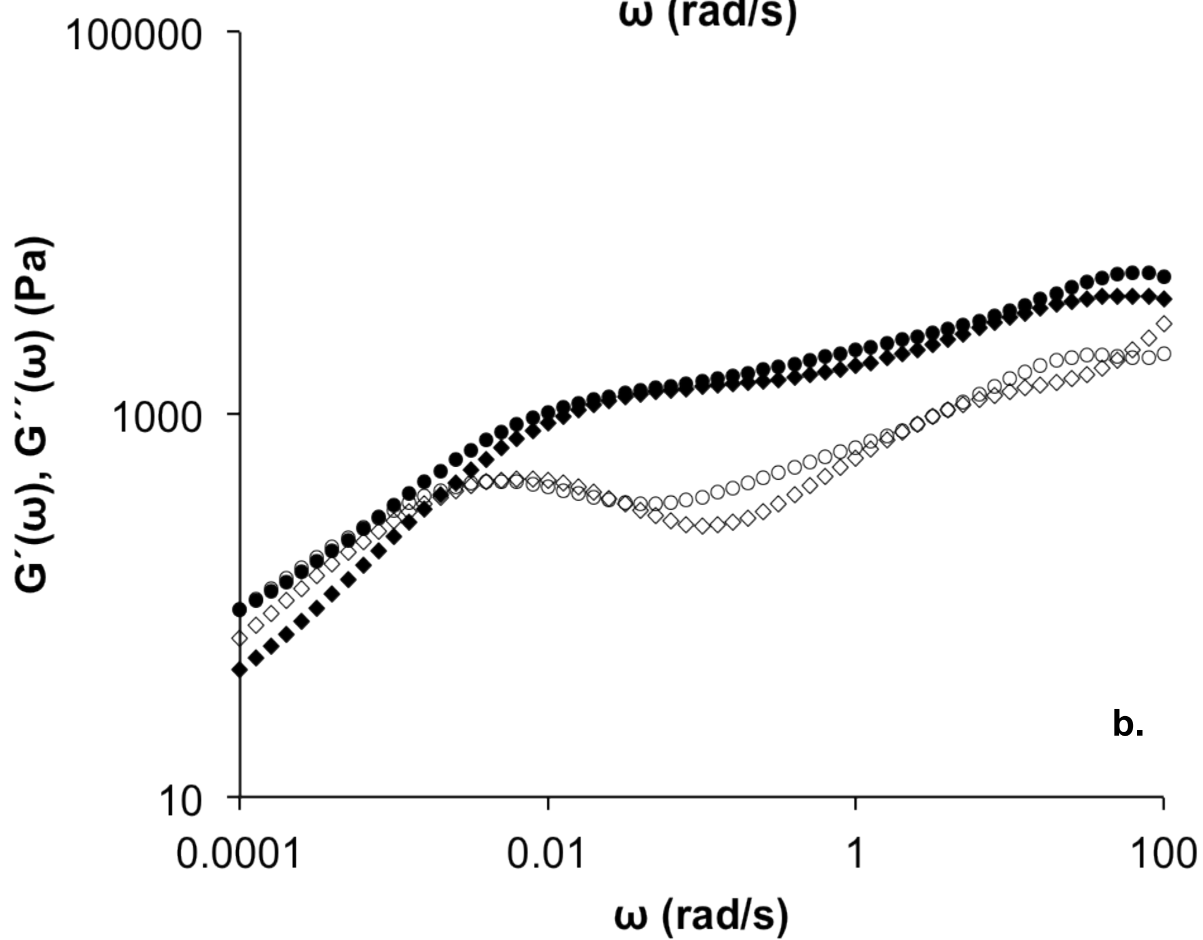
100000
1000
10
0.0001
0.01
1
100
G´(ω), G´´(ω) (Pa)
ω (rad/s)
b.

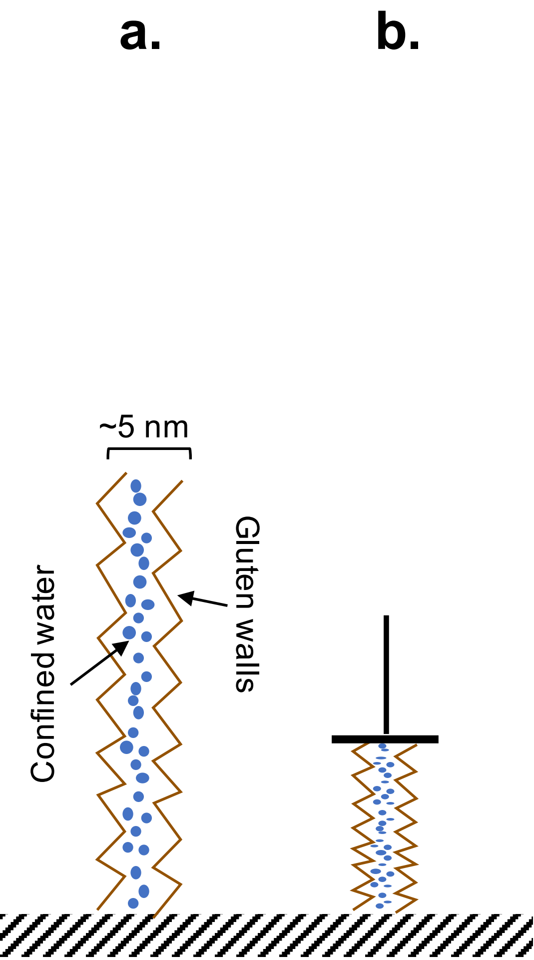

c.
d.
e.

4
3.5
3
2.5

log G(t) (Pa)

0
2
4
6
8

log (t/a_T) (s)